# Doping of hexagonal boron nitride via intercalation: A theoretical prediction

AUTHOR(S):

Oba, Fumiyasu; Togo, Atsushi; Watanabe, Kenji; Taniguchi, Takashi

CITATION:

Oba, Fumiyasu ...[et al]. Doping of hexagonal boron nitride via intercalation: A theoretical prediction. Physical Review B 2010, 81(7): 075125.

ISSUE DATE:

2010-02

URL:

http://hdl.handle.net/2433/126701

PHYSICAL REVIEW B **81**, 075125 (2010)

# Doping of hexagonal boron nitride via intercalation: A theoretical prediction

Fumiyasu Oba* and Atsushi Togo
*Department of Materials Science and Engineering, Kyoto University, Sakyo, Kyoto 606-8501, Japan*

Isao Tanaka
*Department of Materials Science and Engineering, Kyoto University, Sakyo, Kyoto 606-8501, Japan*
*and Nanostructures Research Laboratory, Japan Fine Ceramics Center, Atsuta, Nagoya 456-8587, Japan*

Kenji Watanabe and Takashi Taniguchi
*Advanced Materials Laboratory, National Institute for Materials Science, Tsukuba, Ibaraki 305-0044, Japan*
(Received 12 October 2009; revised manuscript received 27 January 2010; published 26 February 2010)

A doping strategy for hexagonal boron nitride (*h*-BN) is proposed through hybrid Hartree-Fock density functional calculations. Unlike their behavior in typical semiconductors, substitutional dopants generate deep and localized in-gap states in *h*-BN. In contrast, intercalated atoms with high and low electronegativities perturb the host valence and conduction bands weakly, resulting in shallow acceptor and donor states, respectively. The formation of defect complexes involving substitutional dopants suppresses the migration of the intercalated dopants, with the shallow acceptor or donor characteristics preserved. The strategy proposed here is also applicable to *h*-BN ultrathin layers and extendable to the doping of BN single sheets via adsorption.

DOI: 10.1103/PhysRevB.81.075125 PACS number(s): 61.72.Bb, 61.72.J−, 71.55.Eq

## I. INTRODUCTION

Demand for optoelectronic devices in the deep-ultraviolet region has stimulated the exploration of ultrawide-gap semiconductors and the fabrication of their junctions.[1–3] Such examples include the doping of cubic boron nitride (*c*-BN) and ultraviolet light emission from its *p*-*n* junctions.[1,4,5] Recently, a huge exciton binding energy of 0.15 eV and ultraviolet lasing using an electron-beam excitation were observed in another polymorph of BN, the hexagonal phase with a layered structure (*h*-BN).[6,7] Subsequently reported quasiparticle calculations based on the GW and Bethe-Salpeter approaches predicted an even larger binding energy of 0.7 eV.[8,9] The trapping of atoms and molecules on a BN single-sheet nanomesh formed on metal surfaces was also demonstrated recently.[10] These outstanding properties of *h*-BN and related low-dimensional systems can be utilized in wider applications via carrier doping, but it has not yet been reported. In the doping of *h*-BN, a difficulty is expected since even the dopants that have been employed for *c*-BN may not work well due to the characteristic two-dimensional structure. Theoretical modeling should be useful to draw up the guideline for its doping.

In this paper, we propose a strategy for the doping of *h*-BN based on hybrid Hartree-Fock density functional calculations. We show that, unlike their behavior in typical semiconductors including *c*-BN, substitutional impurities yield deep electronic states in *h*-BN. However, the intercalation of suitable impurities in isolated and complex forms, utilizing the large open-space in its layered structure, is effective for both *n*- and *p*-type doping; as a result of a weak perturbation of the host conduction or valence band, shallow donor or acceptor states are generated in *h*-BN with an exceedingly wide band gap of 6 eV. This approach is extendable to the doping of *h*-BN ultrathin layers.

## II. COMPUTATIONAL METHODS

The calculations were performed in the framework of the generalized Kohn-Sham scheme[11] using the plane-wave projector augmented-wave (PAW) method,[12] as implemented in the VASP code.[13–15] The PBE0 hybrid functional,[16–18] which replaces 1/4 of the exchange energy in the Perdew-Burke-Ernzerhof generalized gradient approximation (PBE-GGA) (Ref. 19) with the nonlocal Fock exchange, was employed. PAW data sets with radial cutoffs of 0.9 and 0.8 Å for B and N, respectively, were used with a plane-wave cutoff energy of 400 eV. For impurity calculations, a 288-atom cell was constructed by a $6\times6\times2$ expansion of the primitive cell. Because of the large cell size, only the Γ point was sampled for the Brillouin zone integration, which corresponds to a $6\times6\times2$ *k*-point mesh for the primitive cell. With the cell constants fixed, the internal atomic coordinates were relaxed to reduce the residual forces to less than 0.05 eV/Å; the relaxation of the atoms farthest from the impurity on each BN layer was not allowed in the directions parallel to the layers in order to prevent shearing, i.e., parallel shifts of the layers. Calculations including spin polarization were conducted for selected impurities to test its effects. As a result, we found that the ionization energies of impurities exhibiting deep and localized in-gap states have a tendency to increase by spin polarization, which makes them further unlikely to be effective dopants. On the other hand, impurities with shallow donor or acceptors states, which are the targets of the present study, are almost unaffected. For consistency, the results without spin polarization are presented for all the impurities throughout this paper.

An improved performance of the PBE0 hybrid functional over local and semilocal functionals has been demonstrated for a variety of molecules and solids.[15,17,18,20–23] In particular, the much better reproduction of the band structure for wide-gap systems is notable, and this also holds for *h*-BN. With experimental lattice constants of $a=2.504$ and $c=6.661$ Å,[24]

 

the band gap calculated using PBE0 is 6.28 eV. Those obtained with the local density approximation (LDA) in the Ceperley-Alder form[25] as parameterized by Perdew and Zunger[26] and the PBE-GGA are 4.04 and 4.24 eV, respectively. The PBE0 value is close to the results of quasiparticle calculations, e.g., 5.4,[27] 5.95,[9] 5.99,[8] and 6.03 eV,[28] and also to a recently reported experimental value of 5.971 eV.[6,29] For systems with defects, large differences from the LDA and GGA are expected for PBE0 in the description of localized defect states, but not for shallow donor and acceptor states with a perturbed host band characteristic. In both cases, however, the formation energies calculated using PBE0 can be significantly different from raw or empirically corrected LDA and GGA values because of the discrepancies in the host valence band maximum (VBM) and conduction band minimum (CBM) in addition to the discrepancies in the positions of localized defect states.[22,23,30,31]

Concerning the structural properties, it has been reported that the interlayer interaction in *h*-BN is not well described with the LDA and GGA; a relatively good reproduction with the LDA originates from a cancellation of the errors in the exchange and correlation contributions.[32] In the present study, $a=2.49$ and $c=6.5$ Å with the LDA, and $a=2.51$ and $c=8.0$ Å with the PBE-GGA were obtained, whereas experimental values are $a=2.504$ and $c=6.661$ Å.[24] Similarly to the cases of the LDA and GGA, PBE0 accurately reproduces $a$ (2.50 Å) but not $c$ (7.7 Å). For the impurity supercells, the theoretical value of $a$ was used and the experimental value was taken for $c$. Calculations also performed with the LDA using the theoretical values for both $a$ and $c$ indicated that the formation and ionization energies, and relaxed geometries of the considered impurities are not essentially affected by the choice of the lattice constants.

To evaluate the performance of impurities as donors or acceptors, their formation and ionization energies are used. The former is obtained as[30,31,33,34]

$$E_f = E_T^{\mathrm{imp}} - E_T^{\mathrm{per}} - \sum_i \Delta n_i \mu_i + qE_{\mathrm{F}}, \tag{1}$$

where $E_T^{\mathrm{imp}}$ and $E_T^{\mathrm{per}}$, respectively, denote the total energy of the supercell containing an impurity or its complex in charge state $q$ and that of the perfect-crystal supercell. $\Delta n_i$ is the difference in the number of constituent atoms of type $i$ between these supercells. $\mu_i$ and $E_{\mathrm{F}}$ are the atomic chemical potential and the Fermi level. The reference of $E_{\mathrm{F}}$ was aligned between the impurity and perfect-crystal supercells using their electrostatic potentials.[30,31,33,35] Image charge corrections[36] were not applied since our previous study indicated that for shallow donors and acceptors that weakly perturb the host bands, the neutral states have essentially the same *effective* correction charges as those for the ionized states, and the correction terms are mostly canceled out in the evaluation of ionization energies.[23] In addition, they are unlikely to alter the formation energies obtained using the present 288-atom supercell; the leading correction terms with $L^{-1}$ dependences were estimated to be only ~0.2 eV for singly charged impurities. Corrections for overfilling the conduction band (CB) by donors and for overemptying the valence band (VB) by acceptors in finite-sized supercells[31,33,34] are not required in the case of the 288-atom supercell combined with Γ-only $k$-point sampling because the CBM at the M point and the VBM near the K point are folded onto the Γ point and its immediate vicinity, respectively.

Regarding the atomic chemical potentials, we considered values of $\mu_{\mathrm{B}}$ and $\mu_{\mathrm{N}}$ at the two extreme conditions: the B-rich limit represented by the equilibrium between bulk *h*-BN and B ($\mu_{\mathrm{B}}=\mu_{\mathrm{B(bulk)}}$ and $\mu_{\mathrm{N}}=1/2\mu_{\mathrm{N}_2}+\Delta H_f$) and the N-rich limit represented by the equilibrium between bulk *h*-BN and the $N_2$ molecule ($\mu_{\mathrm{B}}=\mu_{\mathrm{B(bulk)}}+\Delta H_f$ and $\mu_{\mathrm{N}}=1/2\mu_{\mathrm{N}_2}$), where $\Delta H_f$ denotes the formation energy of *h*-BN obtained using PBE0, −2.74 eV. The calculated total energies for the B crystal and the $N_2$ molecule were used for their chemical potentials. Similarly, the chemical potentials of impurity atoms at the impurity-rich limit were determined via equilibrium conditions with relevant simple substances and compounds: for instance, bulk Li, $Li_3N$, $LiN_3$, and $Li_3BN_2$ in the case of the Li impurity. This approximately provides the formation energies at the solubility limit.

The Fermi level at which the formation energies of an impurity or defect in different charge states equalize is referred to as thermodynamical transition level, and its position with respect to the CBM or VBM corresponds to the donor or acceptor ionization energy.[30,31,33,34] The ionization energy is a good measure of the probability of carrier generation, and hence the performance of dopants. In practical doping, the use of nonequilibrium conditions can increase dopant concentrations and thereby overcome high formation energies. Thus, the ionization energy becomes a more important factor, and we primarily base our search for dopants for *h*-BN on the ionization energy.

## III. RESULTS AND DISCUSSION

### A. Substitutional impurities

A natural starting point for our objective, i.e., exploring a doping strategy for *h*-BN, is the investigation of substitutional impurities employed for the doping of *c*-BN: Si and S as donors[1,37] and Be and Mg as acceptors.[4,38] The O impurity, which can be a residual donor in *c*-BN (Refs. 5 and 37) and has been theoretically predicted to have a low formation energy in both *h*- and *c*-BN,[39,40] is also worth consideration. Table I summarizes the calculated ionization energies of the substitutional impurities in *h*-BN. For comparison, those for *c*-BN, which were obtained using 432-atom supercells constructed by a $6\times6\times6$ expansion of the primitive cell and Γ-only $k$-point sampling, are also shown alongside the available experimental values.

For $Be_B$ and $Mg_B$ in *c*-BN, the ionization energies are well reproduced by the present calculations. The theoretical value for $O_N$ is close to the experimental value of 0.32 eV, which has been attributed to either the doped S or residual O impurities.[37] Compared with the case in *c*-BN, the impurities other than O in *h*-BN exhibit much higher ionization energies. This behavior is associated with the formation of deep and localized in-gap states in *h*-BN, as shown later for $S_N$ in Fig. 1(c). Calculations were also conducted for the following

TABLE I. Ionization energies of substitutional impurities in *h*-BN and *c*-BN. The subscript denotes the site of impurities. Values are in eV.

| | | Donor | | | Acceptor | |
|---|---|---|---|---|---|---|
| | | $Si_B$ | $S_N$ | $O_N$ | $Be_B$ | $Mg_B$ |
| *h*-BN | Calc. | 1.19 | 1.22 | 0.33 | 0.53 | 1.45 |
| *c*-BN | Calc. | 0.18 | 0.17 | 0.27 | 0.16 | 0.28 |
| | Exp. | | (0.32)[a] | (0.32)[a] | 0.22[b] | 0.3[c] |

[a]Reference 37. Ionization energy attributed to either S or O.
[b]Reference 38.
[c]Reference 4.

group II, IV, and VI elements at the B and/or N sites, which include those having large size-mismatches: $C_B$, $Ge_B$, $Sn_B$, $Se_N$, and $Te_N$ as donors; and $Ca_B$, $Sr_B$, $Zn_B$, $C_N$, $Si_N$, $Ge_N$, and $Sn_N$ as acceptors. However, all of them were found to have very high ionization energies (>1 eV), originating from deep and localized impurity states. Substitutional dopants are thus unlikely to be effective in *h*-BN.

### B. Intercalation

Another option in the doping of *h*-BN is the incorporation of impurities into the interlayer region. This is referred to as intercalation, especially when a considerable number of atoms or molecules are inserted in layer-structured substances such as graphite. The target of the present work is the dilute intercalation of impurities that act as shallow donors or acceptors. For instance, in the case of *n*-type doping, the band structure needs to be designed as follows: (i) an impurity state appears slightly below the CBM and acts as a shallow donor state, or (ii) an impurity state is distributed within the host bands, and a shallow donor state forms as a consequence of a weak perturbation of the host CB by an impurity potential.[30,41] Although these types of band structure can be attained through covalent bonding interactions between impurity and host orbitals, elements with high valence electron levels, i.e., those with low electronegativities, are often good candidates. Therefore, we chose alkali-metal and alkaline-earth-metal elements. On the basis of a similar consideration, halogen and chalcogen elements with high electronegativities were selected as acceptors.

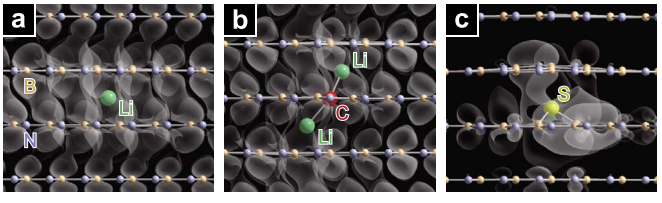


FIG. 1. (Color online). Atomic structure and the squared wave functions of donor states for *h*-BN with neutral impurities: (a) $Li_i$, (b) $2Li_i$-$C_N$, and (c) $S_N$. The isosurfaces of the squared wave functions at $1\times10^{-3}$ Å$^{-3}$ are shown as translucent shapes superposed on the atomic structures viewed along the *a* axis (Ref. 42). Note that the position of $S_N$ has been relaxed significantly toward the interlayer region (upward in this view) from the original N site.

TABLE II. Ionization, formation, and migration energies of intercalated impurities in *h*-BN ($E_i$, $E_f$, and $E_m$, respectively). The complex denotes $2Li_i$-$C_N$, $2Na_i$-$C_N$, or $2F_i$-$C_B$. $E_f$ is evaluated with $E_F=E_{CBM}$ (an *n*-type condition) for the $Li_i$ and $Na_i$ donors and $E_F=E_{VBM}$ (a *p*-type condition) for the $F_i$ acceptor at the B-rich and N-rich limits that provide the lowest $E_f$, respectively. $E_m$ is for ionized impurities in the directions parallel to the BN layers. For the complexes, binding energies for the first and second intercalated impurities with substitutional C are given as $E_b^1$ and $E_b^2$, respectively. Values are in eV.

| | Isolated | | | Complex | | | |
|---|---|---|---|---|---|---|---|
| | $E_i$ | $E_f$ | $E_m$ | $E_i$ | $E_f$ | $E_b^1$ | $E_b^2$ |
| Donor | | | | | | | |
| $Li_i$ | 0.23 | 2.69 | 0.50 | 0.17 | 2.24 | 1.21 | 0.63 |
| $Na_i$ | 0.23 | 3.47 | 0.40 | 0.18 | 4.27 | 1.07 | 0.30 |
| Acceptor | | | | | | | |
| $F_i$ | 0.35 | 4.11 | 0.30 | 0.27 | 4.94 | 1.05 | 0.46 |

An issue of particular concern in the intercalation is that intercalated impurities in the large open space of *h*-BN may be mobile. This is favorable for doping via in-diffusion, but unfavorable in view of the possible electromigration of ionized impurities under an applied electric field. To suppress the migration, trapping by substitutional impurities charged with the opposite sign, i.e., the formation of defect complexes, can be effective. We chose $Be_B$, $C_N$, $C_B$, and $O_N$ since relatively low formation energies were obtained for these substitutional impurities. Complex forms that can be single donors or acceptors were considered on the basis of the valence electronic configurations of the constituent atoms: for example, $2Li_i$-$C_N$, which involves two intercalated Li atoms (single donors) and $C_N$ (single acceptor).

Among the donors considered, the lowest ionization energies were observed for intercalated Li and Na ($Li_i$ and $Na_i$) and their complexes with $C_N$ ($2Li_i$-$C_N$ and $2Na_i$-$C_N$). In the case of the acceptors, $F_i$ and its complex with $C_B$ ($2F_i$-$C_B$) exhibited the lowest values. The properties of these impurities are summarized in Table II. The migration energies of ionized impurities ($E_m$) were evaluated in the directions parallel to the BN layers through the construction of total-energy surfaces with respect to the atomic coordinates of the impurities. As expected from the crystal structure of *h*-BN, the migration perpendicular to the BN layers was found to require very high energies, e.g., 7.2 eV for $Li_i$, and hence is not considered here.

It is noteworthy that the intercalated impurities in both isolated and complex forms have lower ionization energies than any of the substitutional impurities in *h*-BN [Tables I and II]. The analysis of their single-particle electronic structures indicated the formation of a type (ii) band structure in all cases. For instance, $Li_i$ in both isolated and complex forms induces its 2*s* and 2*p* states within the CB (major component) and VB (minor component). The Li-2*s* electron is released to a shallow donor state located slightly below the CBM. As shown in Figs. 1(a) and 1(b), this donor state is characterized as the CB $\pi^*$ orbital with a weak perturbation

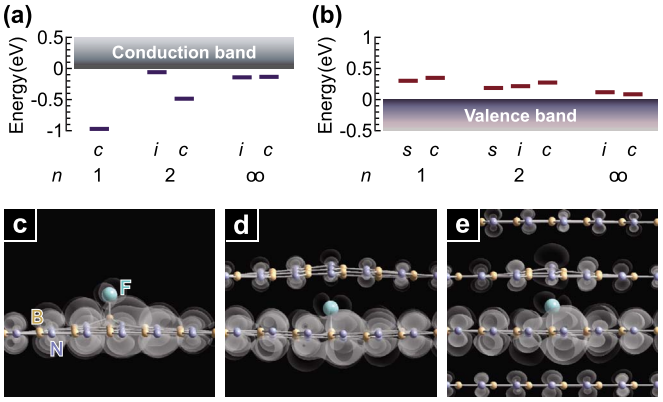


FIG. 2. (Color online) Single-particle energy levels of neutral impurities and their complexes adsorbed on or intercalated in *h*-BN ultrathin layers and crystal (*n*: number of layers): (a) Li-induced donor levels and (b) F-induced acceptor levels. The energies are relative to the CBM or VBM in the corresponding perfect systems. *s*, *i*, and *c* denote the adatom on the surface, the intercalated atom, and the complex, respectively. The atomic structure and the isosurfaces of the squared wave functions of acceptor states are shown in the same manner as that for Fig. 1: (c) $F_s$ on the single sheet ($n=1$), (d) $F_i$ in the bilayer ($n=2$), and (e) $F_i$ in the crystal ($n=\infty$).

by $Li_i$. This is in stark contrast to the case of substitutional S ($S_N$), which yields a deep and localized state [Fig. 1(c)]. For $Na_i$ and its complex, qualitatively the same electronic structures as that for $Li_i$ were observed. In a similar manner, $F_i$ and the $2F_i$-$C_B$ complex induce F-2*p* states mostly within the VB and generate acceptor states that inherit a VB $\pi$-orbital characteristic. As shown later in Fig. 2(e), this state is mainly localized on a neighboring BN layer for isolated $F_i$. On the other hand, it spreads over more than three layers for $2F_i$-$C_B$, suggesting less perturbation of the VB. The corresponding single-particle energy is closer to the VBM, as shown later in Fig. 2(b). The lower ionization energy of $2F_i$-$C_B$ can be attributed to this single-particle electronic structure.

Moving on to the formation energies, $Li_i$ exhibits a much lower value than $Na_i$ at the B-rich limit, as shown in Table II. The equilibrium position for $Li_i$ is located at the center of the BN sixfold rings in the upper and lower layers [Fig. 1(a)]. It is essentially independent of the charge state. The formation energy does not significantly vary with the movement of $Li_i$, yielding a migration energy of 0.50 eV. For the $2Li_i$-$C_N$ complex, the atomic configuration presented in Fig. 1(b) is energetically the most favorable; however, when two of $Li_i$ are placed along *a* axis on the same layer and aligned along *c* axis, the formation energies are only 0.11 and 0.16 eV higher, respectively. The lowest-energy configuration has binding energies of $E_b^1=1.21$ eV for the first $Li_i$ and $E_b^2=0.63$ eV for the second $Li_i$. The formation energy of 2.24 eV is even lower than the value for isolated $Li_i$. At a low temperature and in the presence of $C_N$, $Li_i$ is likely to be trapped by $C_N$ to form the complex. At the same time, the migration of $Li_i$ is hindered, with an effective migration energy of $E_m+E_b^2=1.13$ eV. In contrast to the case of $Li_i$, $F_i$ is bound to a B atom in the neighboring BN layer, as shown later in Fig. 2(e). The migration energy for isolated $F_i$ is as small as 0.30 eV, but $E_b^2=0.46$ eV can serve as an additional barrier due to the complex formation. On the basis of these results, we propose the doping of *h*-BN via intercalation. The complex form is particularly effective when the migration of intercalated dopants must be hindered.

Intercalation and its related functions have been widely studied for graphite. In the case of *h*-BN, intercalation with alkali-metal atoms,[43–45] transition-metal atoms,[46] and molecules such as $Br_2$ (Ref. 44) and $S_2O_6F_2$ (Ref. 47) has been investigated experimentally. However, compared with graphite, available reports on the intercalation are very limited and the structure and properties of intercalated *h*-BN systems are less understood. This is partly due to the difficulty in the intercalation of *h*-BN and the synthesis of its intercalation compounds. Theoretically, Dai and Zhang have suggested the metastability of alkali-metal- or Cu-intercalated *h*-BN compounds through the analysis of vibrational properties using *ab initio* cluster calculations.[48,49] Whereas these experimental and theoretical studies are focused on the intercalation compounds formed as a result of heavy intercalation of *h*-BN, the properties of dilutely intercalated systems have not been explored, in particular with the aim of carrier doping as proposed in the present study.

Concerning the electronic structure of intercalated *h*-BN, Doll *et al.* have reported the optical properties of K-intercalated *h*-BN films with a $C_8K$ graphite intercalation compound-like structure.[45] They found optical absorption with an onset of 2.6 eV and attributed it to electronic transitions between the host and K-induced states. The energy gap associated with host bands was estimated to be 5 eV, which is considerably smaller than the band gap of undoped *h*-BN (5.971 eV).[6] This discrepancy implies that the heavy intercalation that leads to the formation of a BN-K interacted compound alters the band structure of *h*-BN. Our calculation for $(BN)_4K$ with a $C_8K$ structure also found deep K-induced states, in stark contrast to isolated (dilute) $K_i$ yielding a shallow donor state with a perturbed CB characteristic ($E_i=0.30$ eV) as in the aforementioned cases of $Li_i$ and $Na_i$. Thus, the electronic structure is significantly different between dilutely and heavily intercalated *h*-BN. In view of the potential carrier doping that we propose here, experimental investigation of *h*-BN with dilute intercalation is of great interest.

### C. Extension to *h*-BN ultrathin layers

The doping of *h*-BN ultrathin layers is also of fundamental and technological interest. A previous quasiparticle calculation has suggested that a two-dimensional nearly free-electron state constitutes the CBM of the BN single sheet.[27] We observed a similar electronic structure for the BN bilayer, and found that shallow donor states can be induced by intercalation, as in the case of the *h*-BN crystal.

Figures 2(a) and 2(b) show single-particle energy levels of neutral Li, F, and their complexes adsorbed on or intercalated in *h*-BN ultrathin layers ($n=1,2$), alongside those in the *h*-BN crystal ($n=\infty$). The results for the ultrathin layers ($n=1,2$) were obtained using slab models with dimensions of 8*a* and 6*a* along the *a* axis (containing 128 and 144 atoms), respectively, and a vacuum layer thickness of 15 Å.

The donor levels of Li are referenced to the CBM in the corresponding perfect systems and the acceptor levels of F are relative to the VBM. For neutral shallow donors or acceptors, an electron or hole is located at a shallow donor or acceptor state with a perturbed host band characteristic. The effects of such an additional electron and hole on the reference CBM and VBM levels were taken into account as correction terms, which were estimated using the changes in the single-particle levels of the CBM and VBM upon electron addition and removal, respectively. The correction terms are rather large: ~0.4 eV for the CBM and VBM of the *h*-BN perfect-crystal when the 288-atom supercell is used. Those for the ultrathin layers are also ~0.4 eV, which were estimated using a 144-atom *h*-BN perfect-crystal supercell having a similar number of constituent atoms to that of the slab models.

Whereas the ionization energies obtained using total-energy differences via Eq. (1) are presented in Tables I and II, the single-particle energy levels of neutral donors or acceptors are used in Figs. 2(a) and 2(b). They closely reflect the ionization energies when atomic and electronic relaxation by the ionization is small. This typically holds for delocalized and weakly localized states; indeed, the shallow single-particle levels of Li and F in the *h*-BN crystal are qualitatively consistent with their low ionization energies shown in Table II.

Isolated Li atoms are not adsorbed on the surfaces of the single sheet ($n=1$) and the bilayer ($n=2$), and hence the results are not included in Fig. 2(a). In the complex form, they are bound by the mediation of $C_N$, but the resultant levels are 1.0 and 0.5 eV deep from the CBM, respectively. Shallow levels are observed only when the Li atoms are located at the interlayer site: $n \geq 2$ for $Li_i$ (isolated Li), as in the case of the bilayer ($n=2$) shown in Fig. 2(a), and $n \geq 3$ for $Li_c$ ($2Li_i$-$C_N$ complex involving two Li atoms). We found that when an isolated Li atom is merely placed in the electrostatic potential at the interlayer sites of the *h*-BN bilayer and crystal, its occupied 2*s* level is 3.6 and 3.5 eV deep from the CBM, respectively. Therefore, interactions with the host B and N orbitals play an important role in the formation of the shallow donor states. In the case of the *h*-BN crystal, antibonding interactions move the Li-2*s* and -2*p* states above the CBM, leaving a shallow donor state with a weakly perturbed CB characteristic, as mentioned above. For the bilayer, a Li-induced state with a more localized characteristic is generated slightly below the CBM, which corresponds to the shallow donor level for $Li_i$ shown in Fig. 2(a).

In contrast to the behavior of Li, F is strongly bound to a B atom in the single sheet ($n=1$) and at the surface of the bilayer ($n=2$), as well as the case of $F_i$ in the bilayer and crystal [Figs. 2(c)–2(e)]. For the single sheet, a $BN_3F$ tetrahedronlike atomic configuration is observed. As shown in Figs. 2(c)–2(e), the acceptor states of $F_s$ and $F_i$ in all the systems are mainly distributed on one BN layer, but the spatial localization thereon is different. The shallower levels for larger $n$ values can be explained by the less localized characteristic. Thus, the doping strategy using intercalation is applicable to BN systems composed of two or more layers. Moreover, *p*-type doping by F is extendable to the case of BN single sheets. The latter is related to recent reports on BN nanotubes: the synthesis of conducting fluorinated BN nanotubes[50] and first-principles calculations suggesting their *p*-type behavior.[51,52]

## IV. CONCLUSIONS

We propose the bipolar doping of *h*-BN via intercalation based on the hybrid Hartree-Fock density functional calculations. The intercalation of Li, Na, and their complexes leads to the formation of shallow donor states due to a weak perturbation of the CB. The resultant low ionization energies indicate its effectiveness in the *n*-type doping. Similarly, intercalated F and its complex, which induce acceptor states with a perturbed VB characteristic, are suggested to be good acceptors for the *p*-type doping. For these intercalated donors and acceptors, the complex forms are effective particularly when their migration must be suppressed. The strategy proposed here overcomes the expected difficulty in the doping of *h*-BN using substitutional impurities, which exhibit high ionization energies in contrast to the case of *c*-BN. In addition, it is applicable to related low-dimensional systems such as BN single sheets and ultrathin layers.

## ACKNOWLEDGMENTS

This work was supported by Grants-in-Aid for Scientific Research (A), Young Scientists (B), Scientific Research on Priority Areas (No. 474), and a Global COE Program from the MEXT, Japan.

*oba@cms.mtl.kyoto-u.ac.jp

[1] O. Mishima, J. Tanaka, S. Yamaoka, and O. Fukunaga, Science **238**, 181 (1987).
[2] S. Koizumi, K. Watanabe, M. Hasegawa, and H. Kanda, Science **292**, 1899 (2001).
[3] Y. Taniyasu, M. Kasu, and T. Makimoto, Nature (London) **441**, 325 (2006).
[4] M. Lu, A. Bousetta, A. Bensaoula, K. Waters, and J. A. Schultz, Appl. Phys. Lett. **68**, 622 (1996).
[5] T. Taniguchi, K. Watanabe, S. Koizumi, I. Sakaguchi, T. Sekiguchi, and S. Yamaoka, Appl. Phys. Lett. **81**, 4145 (2002).
[6] K. Watanabe, T. Taniguchi, and H. Kanda, Nature Mater. **3**, 404 (2004).
[7] Y. Kubota, K. Watanabe, O. Tsuda, and T. Taniguchi, Science **317**, 932 (2007).
[8] L. Wirtz, A. Marini, M. Gruning, and A. Rubio, arXiv:cond-mat/0508421 (unpublished).
[9] B. Arnaud, S. Lebègue, P. Rabiller, and M. Alouani, Phys. Rev. Lett. **96**, 026402 (2006).
[10] H. Dil, J. Lobo-Checa, R. Laskowski, P. Blaha, S. Berner, J.

Osterwalder, and T. Greber, Science **319**, 1824 (2008).
[11] A. Seidl, A. Görling, P. Vogl, J. A. Majewski, and M. Levy, Phys. Rev. B **53**, 3764 (1996).
[12] P. E. Blöchl, Phys. Rev. B **50**, 17953 (1994).
[13] G. Kresse and J. Furthmüller, Phys. Rev. B **54**, 11169 (1996).
[14] G. Kresse and D. Joubert, Phys. Rev. B **59**, 1758 (1999).
[15] J. Paier, R. Hirschl, M. Marsman, and G. Kresse, J. Chem. Phys. **122**, 234102 (2005).
[16] J. P. Perdew, M. Ernzerhof, and K. Burke, J. Chem. Phys. **105**, 9982 (1996).
[17] C. Adamo and V. Barone, J. Chem. Phys. **110**, 6158 (1999).
[18] M. Ernzerhof and G. E. Scuseria, J. Chem. Phys. **110**, 5029 (1999).
[19] J. P. Perdew, K. Burke, and M. Ernzerhof, Phys. Rev. Lett. **77**, 3865 (1996).
[20] K. N. Kudin, G. E. Scuseria, and R. L. Martin, Phys. Rev. Lett. **89**, 266402 (2002).
[21] J. Paier, M. Marsman, K. Hummer, G. Kresse, I. C. Gerber, and J. G. Ángyán, J. Chem. Phys. **124**, 154709 (2006).
[22] A. Alkauskas, P. Broqvist, and A. Pasquarello, Phys. Rev. Lett. **101**, 046405 (2008).
[23] F. Oba, A. Togo, I. Tanaka, J. Paier, and G. Kresse, Phys. Rev. B **77**, 245202 (2008).
[24] R. S. Pease, Acta Crystallogr. **5**, 356 (1952).
[25] D. M. Ceperley and B. J. Alder, Phys. Rev. Lett. **45**, 566 (1980).
[26] J. P. Perdew and A. Zunger, Phys. Rev. B **23**, 5048 (1981).
[27] X. Blase, A. Rubio, S. G. Louie, and M. L. Cohen, Phys. Rev. B **51**, 6868 (1995).
[28] G. Cappellini, G. Satta, K. Tenelsen, and F. Bechstedt, Phys. Status Solidi B **217**, 861 (2000).
[29] This value has been assigned to a direct gap through the analysis of optical spectra, whereas the present calculations and the reported quasiparticle calculations (Refs. 8, 9, 27, and 28) predict an indirect-type band structure. The interpretation of the optical spectra is controversial (Refs. 53–55).
[30] S. B. Zhang, J. Phys.: Condens. Matter **14**, R881 (2002).
[31] C. Persson, Y.-J. Zhao, S. Lany, and A. Zunger, Phys. Rev. B **72**, 035211 (2005).
[32] A. Marini, P. García-González, and A. Rubio, Phys. Rev. Lett. **96**, 136404 (2006).
[33] C. G. Van de Walle and J. Neugebauer, J. Appl. Phys. **95**, 3851 (2004).
[34] S.-H. Wei, Comput. Mater. Sci. **30**, 337 (2004).
[35] M. Choi, F. Oba, and I. Tanaka, Phys. Rev. B **78**, 014115 (2008).
[36] G. Makov and M. C. Payne, Phys. Rev. B **51**, 4014 (1995).
[37] T. Taniguchi, T. Teraji, S. Koizumi, K. Watanabe, and S. Yamaoka, Jpn. J. Appl. Phys., Part 2 **41**, L109 (2002).
[38] T. Taniguchi, S. Koizumi, K. Watanabe, I. Sakaguchi, T. Sekiguchi, and S. Yamaoka, Diamond Relat. Mater. **12**, 1098 (2003).
[39] W. Orellana and H. Chacham, Phys. Rev. B **62**, 10135 (2000).
[40] T. E. Mosuang and J. E. Lowther, Phys. Rev. B **66**, 014112 (2002).
[41] S. Lany and A. Zunger, Phys. Rev. B **72**, 035215 (2005).
[42] Visualized using the VESTA code (Ref. 56).
[43] A. G. Freeman and J. P. Larkindale, Inorg. Nucl. Chem. Lett. **5**, 937 (1969).
[44] M. Sakamoto, J. S. Speck, and M. S. Dresselhaus, J. Mater. Res. **1**, 685 (1986).
[45] G. L. Doll, J. S. Speck, G. Dresselhaus, M. S. Dresselhaus, K. Nakamura, and S.-I. Tanuma, J. Appl. Phys. **66**, 2554 (1989).
[46] E. Budak and Ç. Bozkurt, J. Solid State Chem. **177**, 1768 (2004).
[47] C. Shen, S. G. Mayorga, R. Biagioni, C. Piskoti, M. Ishigami, A. Zettl, and N. Bartlett, J. Solid State Chem. **147**, 74 (1999).
[48] B.-Q. Dai and G.-L. Zhang, Mater. Chem. Phys. **78**, 304 (2003).
[49] B.-Q. Dai and G.-L. Zhang, Mater. Chem. Phys. **77**, 318 (2003).
[50] C. Tang, Y. Bando, Y. Huang, S. Yue, C. Gu, F. Xu, and D. Golberg, J. Am. Chem. Soc. **127**, 6552 (2005).
[51] H. J. Xiang, J. Yang, J. G. Hou, and Q. Zhu, Appl. Phys. Lett. **87**, 243113 (2005).
[52] H. Liu, G. Zhou, Q. Yan, J. Wu, B.-L. Gu, W. Duan, and D.-L. Zhao, Phys. Rev. B **75**, 125410 (2007).
[53] L. Wirtz, A. Marini, M. Grüning, C. Attaccalite, G. Kresse, and A. Rubio, Phys. Rev. Lett. **100**, 189701 (2008).
[54] B. Arnaud, S. Lebègue, P. Rabiller, and M. Alouani, Phys. Rev. Lett. **100**, 189702 (2008).
[55] K. Watanabe and T. Taniguchi, Phys. Rev. B **79**, 193104 (2009).
[56] K. Momma and F. Izumi, J. Appl. Crystallogr. **41**, 653 (2008).